Journal Pre-proof

Safety estimation for a new model of regenerative and frictional cutting dynamics

Yao Yan, Guojun Liu, Marian Wiercigroch, Jian Xu

PII: S0020-7403(21)00203-4
DOI: https://doi.org/10.1016/j.ijmecsci.2021.106468
Reference: MS 106468

To appear in: *International Journal of Mechanical Sciences*

Received date: 19 January 2021
Revised date: 5 April 2021
Accepted date: 19 April 2021

Please cite this article as: Yao Yan, Guojun Liu, Marian Wiercigroch, Jian Xu, Safety estimation for a new model of regenerative and frictional cutting dynamics, *International Journal of Mechanical Sciences* (2021), doi: https://doi.org/10.1016/j.ijmecsci.2021.106468

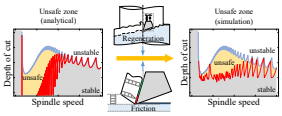

Highlights

- Tool-workpiece friction introduces large-amplitude chatter for unsafe cutting
- Perturbation method is valid for UZ estimation only when friction is neglected
- The cutting safety is estimated by basin stability and Monte Carlo simulation
- The large-amplitude hardly occurs in the unsafe zone from statistical viewpoint

Safety estimation for a new model of regenerative and frictional cutting dynamics

Yao Yan[a], Guojun Liu[b], Marian Wiercigroch[c], Jian Xu[d,*]

[a]*School of Aeronautics and Astronautics, University of Electronic Science and Technology of China, Chengdu, 611731, China*
[b]*Offshore Heavy Industry Design Institute, Shanghai Zhenhua Port Machinery Company Limited (ZPMC), Shanghai, 200125, China*
[c]*Centre for Applied Dynamics Research, School of Engineering, Fraser Noble Building, King's College, University of Aberdeen, Aberdeen, AB24 3UE Scotland, UK*
[d]*Institute of AI and Robotics, Fudan University, Shanghai 200433, China*

Abstract

In our previous discussion on regenerative and frictional cutting dynamics, a new one degree-of-freedom (DOF) model considering both time-delayed regenerative effect in chip thickness and Stribeck effect in frictional velocity as sources of cutting instability has been proposed, which improved the prediction of linear stability in the zone of low cutting velocity. Based on the new model, this investigation focuses on complex nonlinear cutting dynamics. More specifically, the criticality of Hopf bifurcation on the cutting stability boundaries is studied by perturbation analysis, with the co-existence of stationary cutting and chatter obtained in the linearly stable region, i.e., the unsafe zones (UZs) are located for chatter avoidance. Then this analytical estimation is compared with numerical simulations, revealing the possibility of underestimation due to the large-amplitude frictional chatter entering the stable region, which extensively expands the UZs. Beside this local perturbation analysis, global bifurcation diagrams are constructed by numerical simulations, yielding various complex cutting dynamics including multiple stability, regenerative chatter with loss of tool-workpiece contact and stick-slip frictional vibration. Finally, the cutting safety in the UZs is studied based on basin stability estimation, where the functional initial conditions are approximated by Fourier series and chatter occurrence is estimated via Monte Carlo simulation. It is found that from the statistical point of view, the large-amplitude frictional chatter hardly influences the UZs.

Keywords: Cutting process, Regenerative and frictional chatters, Unsafe zones, Complex dynamics, Basin stability.

*Corresponding author. Tel. +86-13611872360, e-mail: jian_xu@fudan.edu.cn

1. Introduction

By considering time-delayed workpiece regeneration [1], velocity-dependent Stribeck friction [2] and process damping [3], the new model improves the prediction of cutting stability, especially in the zone of low cutting velocities. Moreover, the influences of Stribeck effect [4], lubrication [5], rake and shear angles [6] on the stability boundaries have been discussed as well. In [7–11], by introducing new models, the authors tried to bridge the gap in understanding of regenerative and frictional chatters. However, prior to those valuable studies had been being separately performed focusing on individual types of cutting instabilities. As stated in [12], various cutting chatters can be classified into frictional (primary), regenerative (secondary), mode-coupling and thermo-mechanical types, while the primary and secondary have attracted majority of attention from the dynamical systems and manufacturing research communities. For example, the regenerative turning [13], boring [14], milling [15], grinding [16], and drilling [17] chatters attract many attentions while the investigations of frictional types of cutting instabilities in those operations [18–21] are performed simultaneously.

The regenerative chatter theory *blames* a successive regeneration of workpiece surface for the occurrence of secondary chatter [22]. With workpiece material layers being continuously removed by a tool pass in cutting operations, surface profile recording previous tool displacement is generated perturbing the chip thickness for the current tool pass, which introduces time-delayed effects [23, 24], representing the previous tool deformation in the governing equation of cutting dynamics. This regenerative delay varies with the change of spindle rotary velocity, significantly affecting the system's stability [25]. Meanwhile, the cutting stability can also be influenced by frictional effects on the chip-tool interface, especially in the low-velocity zone where negative damping is significant [4]. On the tool-workpiece the primary shear zone is created where the plastically deformed chip sticks to the tool tip before slides along the tool's rake surface, yielding complex velocity-dependent frictional interactions [5, 26]. This effect plays the role of negative damping, leading to non-smoothness frictional chatter with stick-slip motion [2, 19]. To avoid this scenario, one can increase the spindle rotary speed to weaken the Stribeck effect [27]. Beside the two sources of cutting instability, contact between tool's flank surface and wavy workpiece surface introduces process damping inversely proportional to cutting velocity, expanding the stable region in the low-velocity zone [3, 28, 29].

By using the dynamic model described above, a good prediction of the linear cutting stability can be obtained [7]. However, it has been gradually realized in the past decade, the linear analysis alone is insufficient for guaranteeing the cutting stability due to multi-stability introducing large-amplitude chatter into linearly stable regions, making them unsafe [30]. The unsafe cutting (UC) was postulated

by Stépán [13], who showed that the global stability of stationary cutting can only be guaranteed when system parameters are chosen to be 8-10% below the linear stability limit. Insperger *et al.* in [31] supported this hypothesis with the theory of subcritial Hopf bifurcation, which generates a branch of unstable periodic solution on the stability boundaries bending towards the linearly stable region until it reaches loss of tool-workpiece contact for stable chatter. Based on this concept, the cutting multi-stability and its corresponding unsafe zones (UZs) can be estimated [1, 32–34].

Then the discussion on UC was extended by Yan *et al.* [35], who estimated the cutting safety in the UZs to predict the possibility of chatter occurrence. Multi-stability in ordinary differential systems are normally studied by basin of attraction or basin stability, which sweeps the spaces of potential initial conditions and tracks their trajectories towards each attractors [36]. However, this method is cumbersome for time-delayed systems, which have infinite many dimensions as their initial conditions are defined in functional spaces [37]. To solve this problem for the estimation of basin of attraction or basin stability of delayed systems, one has to map the infinite many dimensions onto some finite dimensional spaces. Possible solutions are artificially cutting off delayed control signals at the very beginning [38], assuming constant functional initial conditions [39], using polynomials [40] or orthogonal bases [41] for approximation, etc. Given the periodic property of workpiece surface, Yan *et al.* [35] used Fourier series to approximate the functional initial conditions of a regenerative turning process, with the basin stability estimated to discuss the influences of surface waviness, cutting geometry and tool deflection on the cutting safety. Recently, this method was further extended by Yan *et al.* [42], who combines Fourier series and Monte Carlo principle for a better approximation of various types of wavy workpiece surface.

Based on the new model proposed in [7], the rest of this paper focuses on nonlinear cutting dynamics involving both regenerative and frictional effects. Firstly, the model with its prediction of linear stability is briefly revisited in Section 2. Then Section 3 employs both the perturbation analysis and numerical simulations to locate the UZs, revealing that the estimation by perturbation methods could be invalid, especially when the bifurcation pattern is dominated by frictional chatter with large amplitudes. After that, the cutting safety is evaluated based on approximation of functional initial conditions with Fourier series and Monte Carlo principle in Section 4, which unveils that the large-amplitude frictional chatter does not expand the UZ from statistical viewpoint. Finally, some conclusions are drawn in Section 5.

2. Revisiting of the new model

An orthogonal cutting which occurs in a typical turning operation is illustrated in Fig. 1, with the cutting zone enlarged to show the details of tool-workpiece interaction. As the workpiece rotates with an spindle speed N [r min^{-1}], the material is fed into the cutting tool with a workpiece speed $V_c = \frac{R\pi N}{30}$

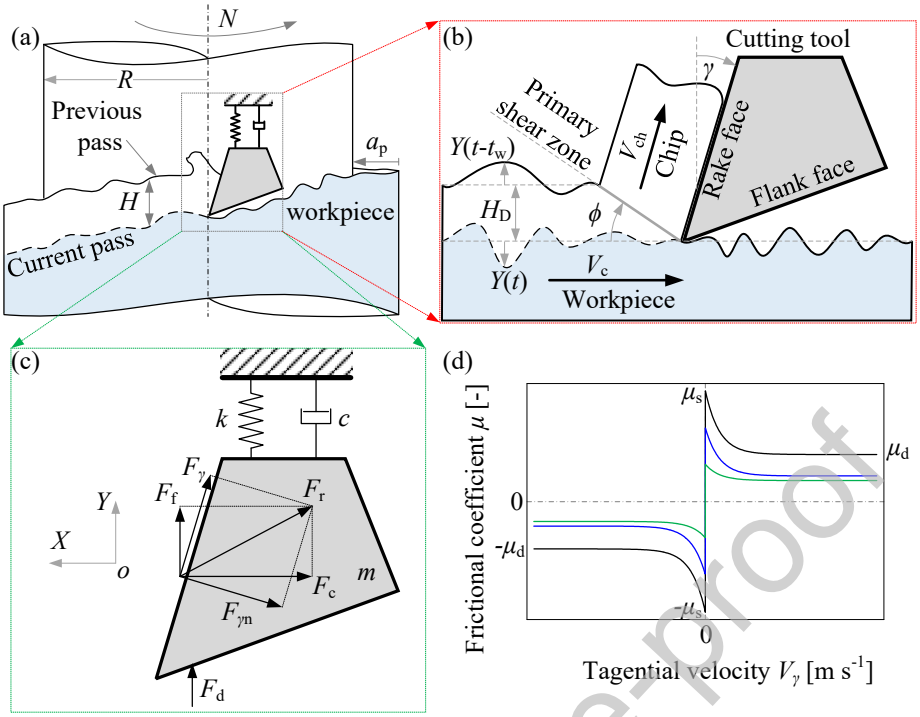

Figure 1: (a) Regenerative cutting operation, where (b) the chip flows along the tool's rake surface and the uncut workpiece is compressed by the tool tip. (c) Cutting and feeding forces are generated by chip-tool interaction on the rake surface, and process damping force is exerted by the workpiece on tool's flank surface. (d) Stribeck effect in the chip-tool friction for different workpiece materials [7, 8].

[m s^{-1}], where R [m] is the workpiece radius. In the primary shear zone [12], the material to be removed is deformed to be chips flowing along the tool's rake surface, exerting horizontal cutting and vertical feeding forces, F_c [N] and F_f [N], on the tool's rake face. Meanwhile, the uncut material flow along the tool's flank surface, introducing a process damping force, F_d [N], in Y-direction [3].

2.1. Modelling of regenerative and frictional cutting dynamics

The vertical response of the tool displayed in Fig. 1(c) is governed by

$$m\ddot{Y}(t) + c\dot{Y}(t) + kY(t) = F_f + F_d, \tag{1}$$

where m [kg], c [N s m^{-1}] and k [N m^{-1}] are equivalent mass, damping and stiffness of the cutting tool. In Eq. (1), the dots over Y represent derivatives of Y with respect to time t [s]. The process damping force can be expressed as [3, 29]

$$F_d = C_y a_p \frac{\dot{Y}(t)}{V_c}, \tag{2}$$

where C_y [N m^{-1}] and a_p [m] are process damping coefficient and radial depth of cut, respectively. The feeding force consists of Y-components of both normal and tangential tool face forces, $F_{\gamma n}$ and F_γ.

The simplest model of the normal force, $F_{\gamma \mathrm{n}}$ can be represented as follows [8, 28, 43]:

$$F_{\gamma \mathrm{n}} = K a_{\mathrm{p}} H(t), \tag{3}$$

where K [N m^{-2}] and $H(t)$ [m] are cutting force coefficient and and chip thickness, respectively. According to the regenerative theory shown in Fig. 1(a), the upper and lower surfaces of the chip are respectively generated by previous and current tool passes, yielding the following instantaneous chip thickness [35]

$$H(t) = H_{\mathrm{D}} - Y(t) + Y(t - t_{\mathrm{w}}), \tag{4}$$

where H_{D} [m] and $t_{\mathrm{w}} = \frac{60}{N}$ [s] are nominal chip thickness and rotational period of the workpiece, respectively. The normal force, $F_{\gamma \mathrm{n}}$, also induces tangential frictional force expressed as

$$F_{\gamma} = \mu F_{\gamma \mathrm{n}}, \tag{5}$$

where μ is equivalent frictional coefficient shown in Fig. 1(d). It is velocity-dependent expressed as [6, 26, 44–46]

$$\mu = \mathrm{sign}(V_{\gamma}) \left(\mu_{\mathrm{d}} + (\mu_{\mathrm{s}} - \mu_{\mathrm{d}}) \exp\left(-\frac{|V_{\gamma}|}{V_{\mathrm{s}}} \right) \right), \tag{6}$$

where V_{γ} [m s^{-1}] and V_{s} [m s^{-1}] are frictional chip velocity relative to the tool and Stribeck velocity, and μ_{s} and μ_{d} are static and dynamic coefficients of friction, respectively [20, 47].

Given the tool geometry and chip movement, the feeding force and the frictional velocity of the chip along the rake face can be represented as

$$F_{\mathrm{f}} = F_{\gamma} \cos(\gamma) - F_{\gamma \mathrm{n}} \sin(\gamma). \tag{7}$$

and

$$V_{\gamma} = V_{\mathrm{ch}} - \dot{Y}(t) \cos(\gamma), \tag{8}$$

where V_{ch} [m s^{-1}] and γ are the chip velocity and the rake angle of the tool shown in Fig. 1(b). By applying the mass conservation principle in the primary shear zone, one obtains the chip velocity as follows

$$V_{\mathrm{ch}} = V \frac{\sin(\phi)}{\cos(\phi - \gamma)}, \tag{9}$$

where ϕ is the shear angle displayed in Fig. 1(b) [12].

The above model can be nondimensionalized for further linear and nonlinear analyses by introducing

the following dimensionless parameters [35, 48]

$$\begin{aligned}
&\xi = \frac{c}{\sqrt{mk}}, \quad w = a_{\mathrm{p}}\frac{K}{k}, \quad v_{\mathrm{s}} = \frac{30V_{\mathrm{s}}\cos(\gamma-\phi)}{\pi R\sin(\phi)}\sqrt{\frac{m}{k}}, \quad c_y = \frac{30C_y}{\pi RK},\\
&\nu = \frac{H_{\mathrm{D}}}{V_s}\sqrt{\frac{k}{m}}, \quad n = N\sqrt{\frac{m}{k}}, \quad \tau_{\mathrm{w}} = \frac{60}{n} = t_{\mathrm{w}}\sqrt{\frac{k}{m}}, \quad \Omega = \frac{2\pi}{\tau_{\mathrm{w}}},
\end{aligned} \tag{10}$$

and variables:

$$\begin{aligned}
&\tau = t\sqrt{\frac{k}{m}}, \quad y_1(\tau) = \frac{Y(t)}{H_{\mathrm{D}}}, \quad y_2(\tau) = y_1'(\tau) = \frac{\dot{Y}(t)}{H_{\mathrm{D}}}\sqrt{\frac{m}{k}}\\
&h(\tau) = \frac{H(t)}{H_{\mathrm{D}}} = 1 - y_1(\tau) + y_1(\tau-\tau_{\mathrm{w}}),\\
&v_\gamma(\tau) = \frac{V_\gamma}{H_{\mathrm{D}}}\sqrt{\frac{m}{k}} = \frac{n}{v_{\mathrm{s}}} - \nu\cos(\gamma)y_2(\tau).
\end{aligned} \tag{11}$$

Then the governing equation is changed into a set of first order ODEs as follows

$$\begin{aligned}
&y_1'(\tau) = y_2(\tau),\\
&y_2'(\tau) = -y_1(\tau) - \xi y_2(\tau) + w\left(\mu\cos(\gamma) - \sin(\gamma)\right)h(\tau) - wc_y\frac{y_2(\tau)}{n},
\end{aligned} \tag{12}$$

with

$$\mu = \mathrm{sign}(v_\gamma)\left(\mu_{\mathrm{d}} + (\mu_{\mathrm{s}} - \mu_{\mathrm{d}})\exp\left(-|v_\gamma|\right)\right). \tag{13}$$

The prime over $y_1(t)$ and $y_2(t)$ in Eqs (11) and (12) represents the derivative with respect to the dimensionless time, τ.

2.2. Linear stability analysis of the cutting process

For a stationary cutting without oscillation in the tool's deformation, $(y_1(\tau), y_2(\tau)) \equiv (y_{10}, 0)$, Eq. 12 yields

$$y_{10} = w\left(\mu_{\mathrm{d}} + (\mu_{\mathrm{s}} - \mu_{\mathrm{d}})\exp\left(\frac{n}{v_{\mathrm{s}}}\right)\right)\cos(\gamma) - w\sin(\gamma). \tag{14}$$

This steady state represents a stable cutting operation when the linear part of Eq. (12),

$$\mathbf{y}'(\tau) = \mathbf{A}\mathbf{y}(\tau) + \mathbf{D}\mathbf{y}(\tau-\tau_{\mathrm{w}}), \tag{15}$$

has a stable equilibrium [20]. The vector and coefficient matrices in Eq. (15) are as follows

$$\mathbf{y}(\tau) = \begin{pmatrix} y_1(\tau) - y_{10} \\ y_2(\tau) \end{pmatrix}, \quad \mathbf{A} = \begin{pmatrix} 0 & -1 \\ 1+wa & \xi+wb \end{pmatrix}, \quad \mathbf{D} = \begin{pmatrix} 0 & 0 \\ -wa & 0 \end{pmatrix}, \tag{16}$$

where

$$\begin{aligned} a &= \left(\mu_{\mathrm{d}} + (\mu_{\mathrm{s}} - \mu_{\mathrm{d}}) \exp\left(-\frac{n}{v_{\mathrm{s}}}\right)\right) \cos(\gamma) - \sin(\gamma), \\ b &= \frac{c_y}{n} + (\mu_{\mathrm{d}} - \mu_{\mathrm{s}}) \nu \cos^2(\gamma) \exp\left(-\frac{n}{v_{\mathrm{s}}}\right). \end{aligned} \tag{17}$$

The linear stability is mathematically determined by the eigenvalues of Eq. (15), i.e., the solutions of the following eigenvalue equation [49]

$$\det(\lambda \mathbf{I} - \mathbf{A} - \mathbf{D} \exp(-\lambda \tau_{\mathrm{w}})) = 0, \tag{18}$$

where det() and λ represent the determinant and eigenvalues, respectively. A stable equilibrium requires all the eigenvalues having negative real parts, but any λ with positive real part destabilises the stationary cutting. Thus the critical stability corresponds with a pair of imaginary eigenvalues, $\lambda = \pm \mathrm{i}\omega$, which changes Eq. (18) into [35]

$$\det(\mathrm{i}\omega \mathbf{I} - \mathbf{A} - \mathbf{D} \exp(-\mathrm{i}\omega \tau_{\mathrm{w}})) = 0, \tag{19}$$

or

$$\begin{aligned} \omega^2 - 1 - wa(1 - \cos(\omega \tau_{\mathrm{w}})) &= 0, \\ (\xi + wb)\omega - wa \sin(\omega \tau_{\mathrm{w}}) &= 0. \end{aligned} \tag{20}$$

From Eq. (17), it is known that a and b depend on $n = \frac{60}{\tau_{\mathrm{w}}}$, making Eq. (20) transcendental for its analytical solution (see [32] for a less involved problem). Therefore the following analysis will use a numerical method based on the Newton-Raphson iteration method and continuation scheme for the cutting stability (see more details in Appendix A [20]).

2.3. A case study

This new model can be validated by comparing the stability diagram with the one obtained by Altintas et al. [3] and Eynian [50]. They used a carbide grooving tool with 2.4 [mm] clearance edge with 0° rake angle to cut a turning cold rolled AISI 1045 steel workpiece with a diameter of 30 [mm]. According to their identification, the cutting process is of the parameter values as follows

$$\begin{aligned} &m = 0.561 \text{ [kg]}, \quad c = 145 \text{ [N s m}^{-1}\text{]}, \quad k = 6.48 \times 10^6 \text{ [N m}^{-1}\text{]}, \\ &K = 6.02 \times 10^9 \text{ [N m}^{-2}\text{]}, \quad C_y = 6.11 \times 10^5 \text{ [N m}^{-1}\text{]}, \\ &R = 0.0175 \text{ [m]}, \quad H_{\mathrm{D}} = 0.0005 \text{ [m]}, \quad \gamma = 0 \text{ [degree]}, \quad \phi = 45 \text{ [degree]}. \end{aligned} \tag{21}$$

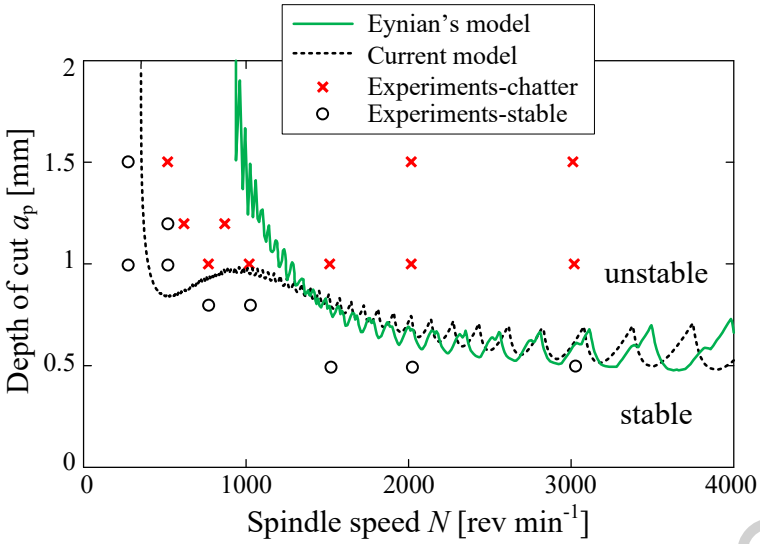

Figure 2: Stability boundaries (dashed black) obtained by numerical solving Eq. (20), compared with the green solid curve from Eynian's model and the experimental results in [50] marked by black circles (stable) and red crosses (unstable).

In the analysis of cutting stability, they considered the regenerative effect and process damping in the tool-workpiece interface, without considering the Stribeck frictional force. As seen in Fig. 2, the original boundary failed to discriminate the chatter from the stationary cutting in the low-velocity region. To improve the stability analysis, we consider the frictional effect while adopting the above parameters.

However, there is no identification of frictional coefficient between carbide tools and cold rolled AISI 1045 steel to the best of the authors' knowledge. Thus, we use the equivalent frictional coefficient between a carbide tool and cold AISI 4140 steel which was identified by Claudin et al. [51]. The fitted coefficient of Eq. (6) are listed as follows [7]

$$V_s = 0.65 \text{ [m s}^{-1}\text{]}, \quad \mu_d = 0.23, \quad \mu_s = 0.54, \tag{22}$$

and

$$\xi = 0.07605, \quad v_s = 0.10436, \quad \nu = 2.61434, \quad c_y = 0.05541. \tag{23}$$

With the above values, Eq. (20) yields the dashed black curves in Fig. 2 for the stability limit, which is in accordance with the experimental results in [50].

3. Unsafe zones

In addition to the linear cutting stability, it has been gradually realized in the last decade that the nonlinearity in the cutting force also crucially affects the cutting dynamics in the neighbourhood

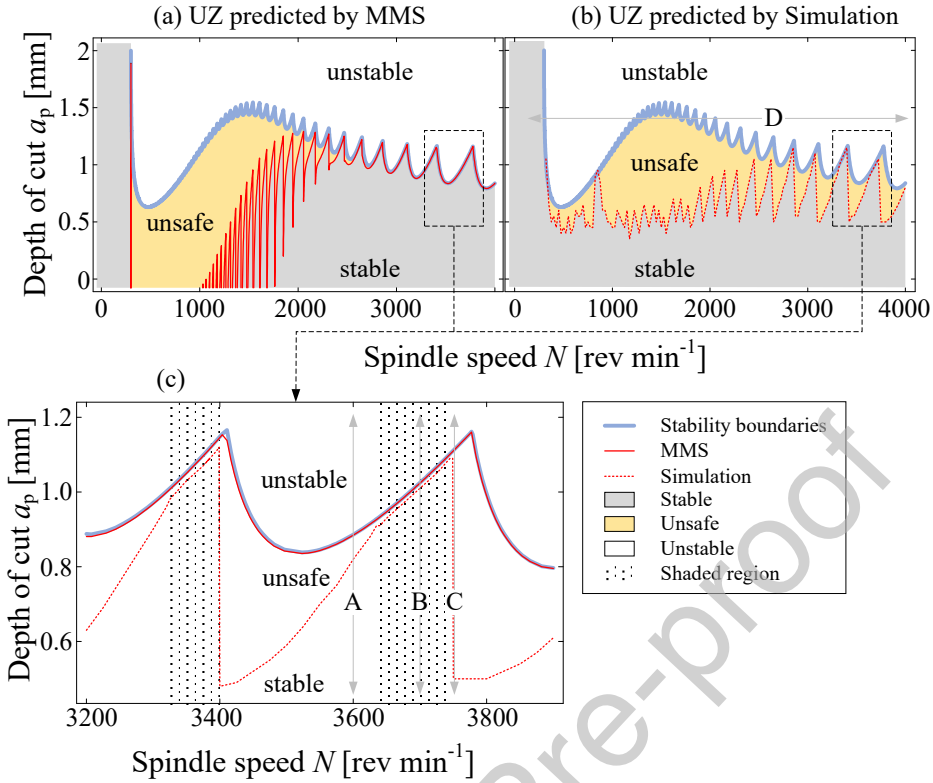

Figure 3: Unsafe zones predicted by (a) analytical estimation with MMS and (b) numerical simulations, where the stability limit corresponds with the last result in [7]. (c) The region for $N \in [3200, 3900]$ [rev min^{-1}] is enlarged for the comparison of the two results where only the estimation in the shaded regions ($N \in [3325, 3339]$ [rev min^{-1}] and $N \in [3640, 3749]$ [rev min^{-1}]) are qualitatively correct.

of the stability boundaries, which introduces multi-stability to deteriorate the linear cutting stability [31, 32, 34, 35]. Due to the uncertainty of cutting dynamics induced by this multi-stability, such scenarios are deemed as unsafe cutting (UC) and the regions are unsafe zones (UZs) [1]. As claimed by Insperger *et al.* [31], typical UZs are introduced by subcritical instability on stability boundaries, which yields a branch of unstable periodic orbit bending into the stable region until the cutting tool loses its contact with the workpiece for stable chatter orbit. Therefore, the UZs can be estimated by using perturbation method, tracking the unstable periodic orbit and checking its non-smoothness.

Based on this theory, the method of multiple scales (MMS) is employed to estimate the UZs illustrated in Fig. 3(a), where the angles are chosen as $\gamma = 4°$ and $\phi = 40°$ corresponding with the last result given in [7]. More details of the MMS analysis can be found in Appendix B or Refs [52, 53]. However, this analytical estimation has a discrepancy when compared with the numerical result presented in Fig. 3(b). More specifically, the analytical result underestimates the UZ in the high-velocity zone but overestimates it in the low-velocity zone. In addition, as depicted in the blown-up window in Fig. 3(c), the analytical estimation is qualitatively correct only in the shaded regions, but fail to predict the UZs in the other

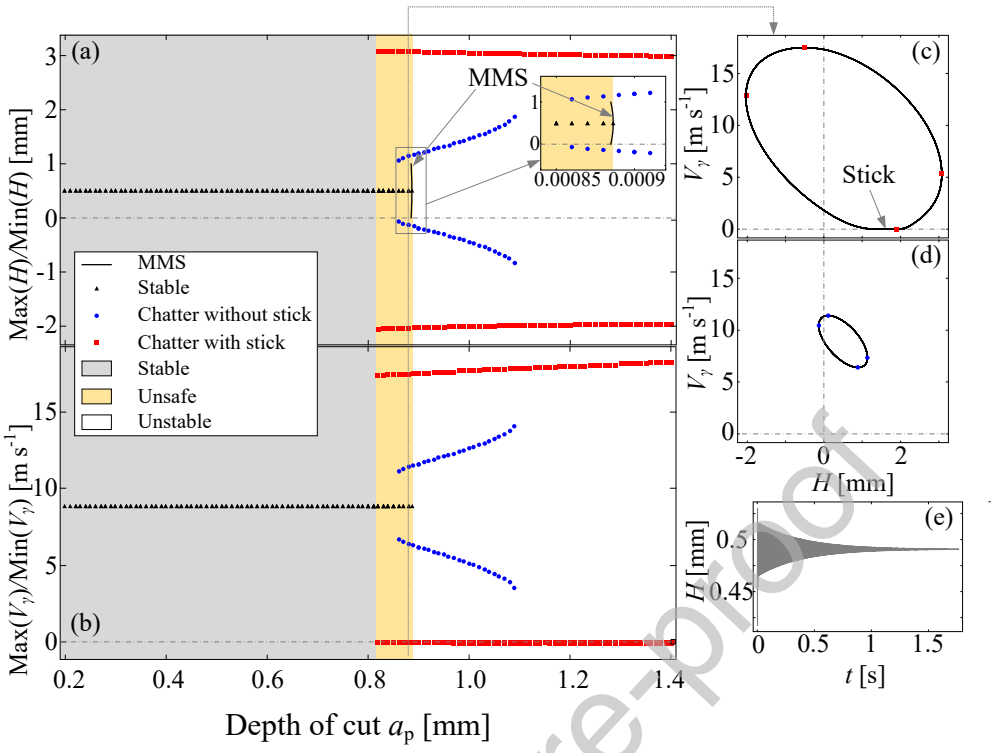

Figure 4: Bifurcation diagrams of (a) chip thickness H and (b) frictional velocity V_γ as functions of the depth of cut a_p for $N = 3600$ [rev min^{-1}], with phase portraits of (c) large-amplitude frictional and (d) small-amplitude chatters and (e) time series of stationary cutting for $a_\mathrm{p} = 0.88$ [mm] added. Linearly, the stationary cutting should be stable in both the grey and yellow regions, but the cutting safety in the yellow region is deteriorated as the stationary cutting may jump to the large-amplitude frictional chatter in Panel (c) under unexpected external perturbations. As a result, the available depth of cut and its corresponding efficiency are decreased by this multi-stability.

regions. To demonstrate the difference, we consider three different speeds of $N = 3600$ [rev min^{-1}], 3700 [rev min^{-1}] and 3750 [rev min^{-1}] marked as A B and C in Fig. 3 for further bifurcation analyses.

To begin with, the bifurcation diagrams for speed A ($N = 3600$ [rev min^{-1}]) are constructed in Fig. 4, with the minimum and maximum values of H and V_γ plotted as functions of the depth of cut a_p. With respect to the increase of a_p, the stationary cutting is globally stable until a_p reaches 0.82 [mm] where a large-amplitude chatter marked by red squares turns up to co-exists with the stable cutting, so that the grey stable region is transformed into the yellow UZ. When a_p further increases to 0.86 [mm], as seen in the small blown-up window, another small-amplitude chatter marked by blue dots shows up for tristability. The stable cutting then disappears for $a_\mathrm{p} \geq 0.89$ [mm] where the cutting process enters the unstable region. Thereafter, two kinds of cutting chatters co-exist until a_p reaches 1.1 [mm], where the small-amplitude one disappears, leaving only the stronger vibration. For a clear observation of these cutting dynamics, phase portraits and time series for $a_\mathrm{p} = 0.88$ [mm] are illustrated in Figs 4(c), (d) and (e). It is seen that the large-amplitude chatter in Fig 4(c) has a sticking phase ($V_\gamma = 0$), which is a typical characteristic of frictional chatter. By contrast, the small-amplitude chatter has non-smoothness

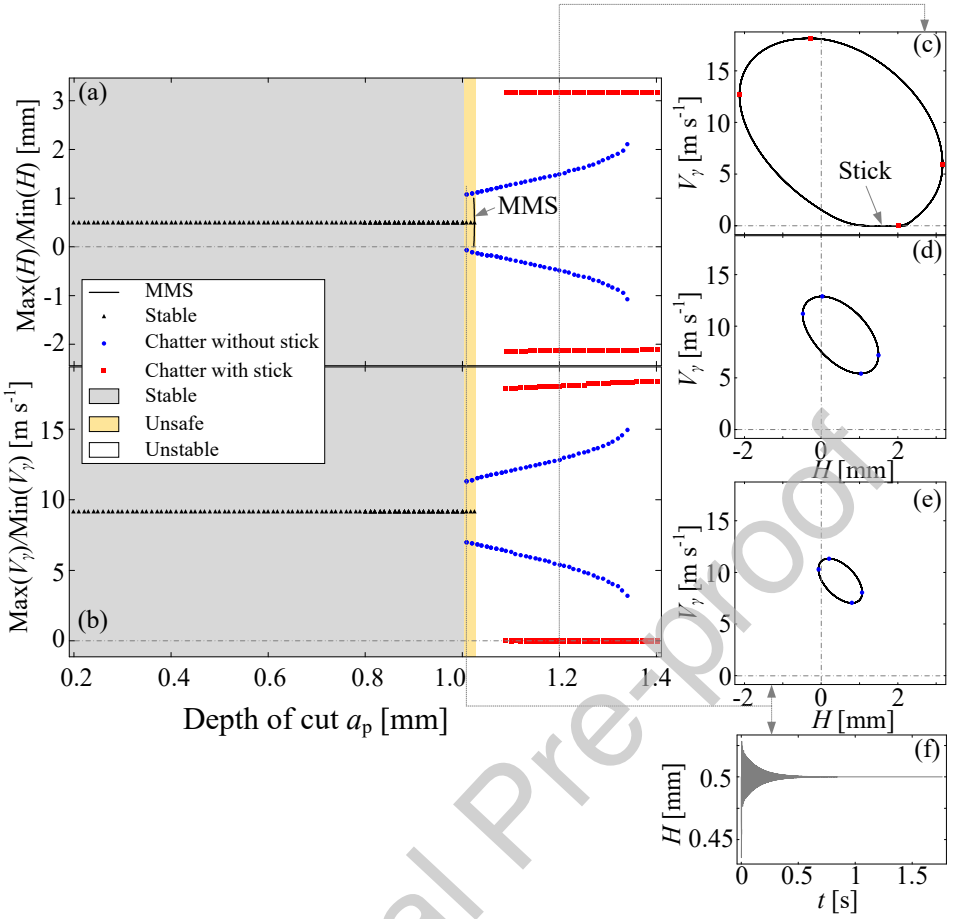

Figure 5: Bifurcation diagrams of (a) chip thickness H and (b) frictional velocity V_γ as functions of the depth of cut a_p for $N = 3700$ [rev min^{-1}], with phase portraits of (c) large-amplitude frictional and (d) small-amplitude regenerative chatters for $a_\mathrm{p} = 1.01$ [mm] and (e) phase portrait of small-amplitude regenerative chatter and (f) time series of stationary cutting for $a_\mathrm{p} = 0.88$ [mm] added. The UZ is relative small and influenced only by the small-amplitude regenerative chatter, yielding the most accurate estimation of UZ by the MMS.

only in the cutting depth H, indicating a regenerative chatter.

The bifurcation diagram in Fig. 4 reminds us that the discrepancy between the analytical and numerical estimations is originated from the branch of large-amplitude frictional chatter which is beyond the capability of local perturbation methods. This assumption can be validated by the bifurcation diagram for speed B ($N = 3700$ [rev min^{-1}]) in Fig. 5, where the MMS yields a much better estimation. As seen, the UZ for $a_\mathrm{p} \in [1.01, 1.03]$ [mm] in Fig. 5 is much smaller than that in Fig. 4 as it is determined only by the small-amplitude chatter and the non-smoothness in the cutting depth ($H \leq 0$). The large-amplitude chatter with sticking phases ($V_\gamma = 0$) is absent until a_p is increased for the coexistence of two chatters for $a_\mathrm{p} \in [1.09, 1.34]$ [mm]. As the frictional chatter does not affect the UZ, this case is in accordance with the theory proposed by Insperger *et al.* [31], so that the estimation is qualitatively correct. In application, this case is more reliable as it has the smallest UZ for the avoidance of cutting chatter from the global

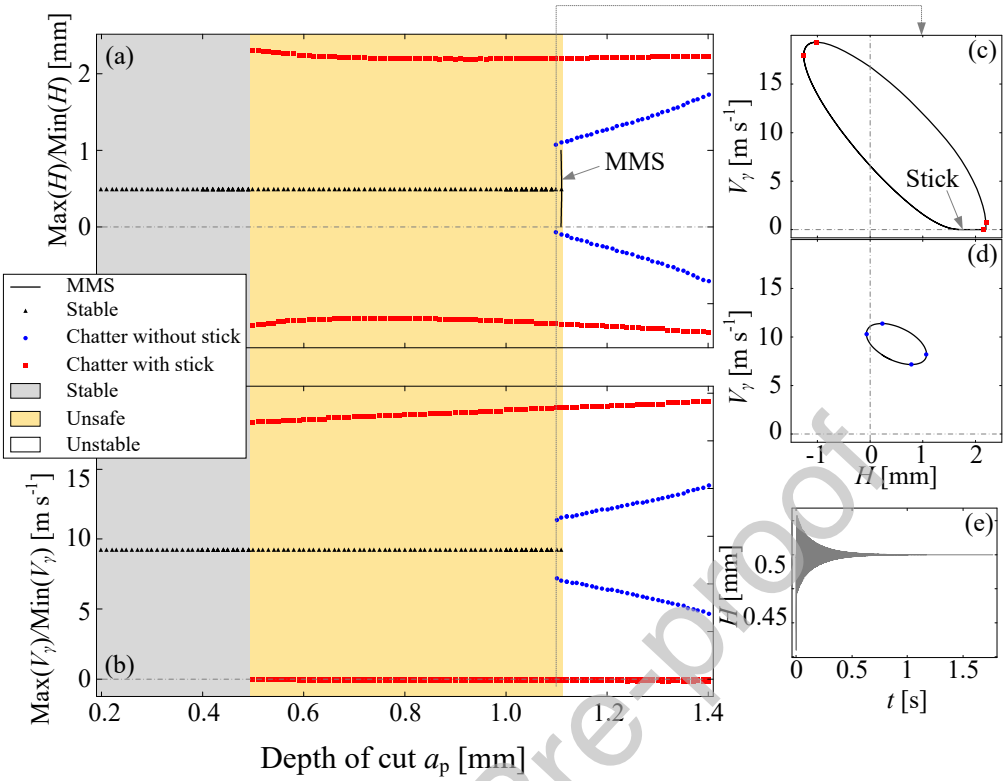

Figure 6: Bifurcation diagrams of (a) chip thickness H and (b) frictional velocity V_γ as functions of the depth of cut a_p for $N = 3750$ [rev min^{-1}], with phase portraits of (c) large-amplitude frictional and (d) small-amplitude chatters, and (e) time series of stationary cutting for $a_\mathrm{p} = 1.1$ [mm] added. The large-amplitude frictional chatter has a crucial influence on the cutting multi-stability, which yields a very large UZ and extensively deteriorates the cutting efficiency as the depth of cut should be very small ($a_\mathrm{p} < 0.5$ [mm]) for chatter avoidance. Therefore, the spindle speed in application should be in the shaded regions depicted in Fig. 3 for deep cutting.

viewpoint.

When N further grows to 3750 [rev min^{-1}], which corresponds to C beyond the shaded region in Fig. 3, the bifurcation diagrams are suddenly dominated by the large-amplitude frictional chatter, yielding a very large UZ in Fig. 6. Based on the analytical estimation, the UZ is supposed to have a very small span, $a_\mathrm{p} \in [1.2, 1.21]$ [mm]. However, the large-amplitude frictional chatter with sticking phase begins to co-exist with the stable stationary cutting for $a_\mathrm{p} = 0.5$ [mm], which extensively expands the UZ to be $a_\mathrm{p} \in [0.5, 1.21]$ [mm]. Therefore, the perturbation method without considering the large-amplitude frictional chatter underestimates the UZ in the high-velocity zone in Fig. 3.

The difference between the UZs in Figs 5 and 6 is significantly influenced by the large-amplitude frictional chatter, indicating a sudden switch between two distinct vibrations. To reveal the mechanism and study the influence of spindle speed on the cutting dynamics, next bifurcation analysis is performed along D marked in Fig. 3 for $a_\mathrm{p} = 1.4$ [mm] and $N \in [200, 4000]$ [rev min^{-1}]. Corresponding bifurcation diagrams of H and V_γ are displayed as functions of N in Figs 7(a) and (b), where the blue dots and

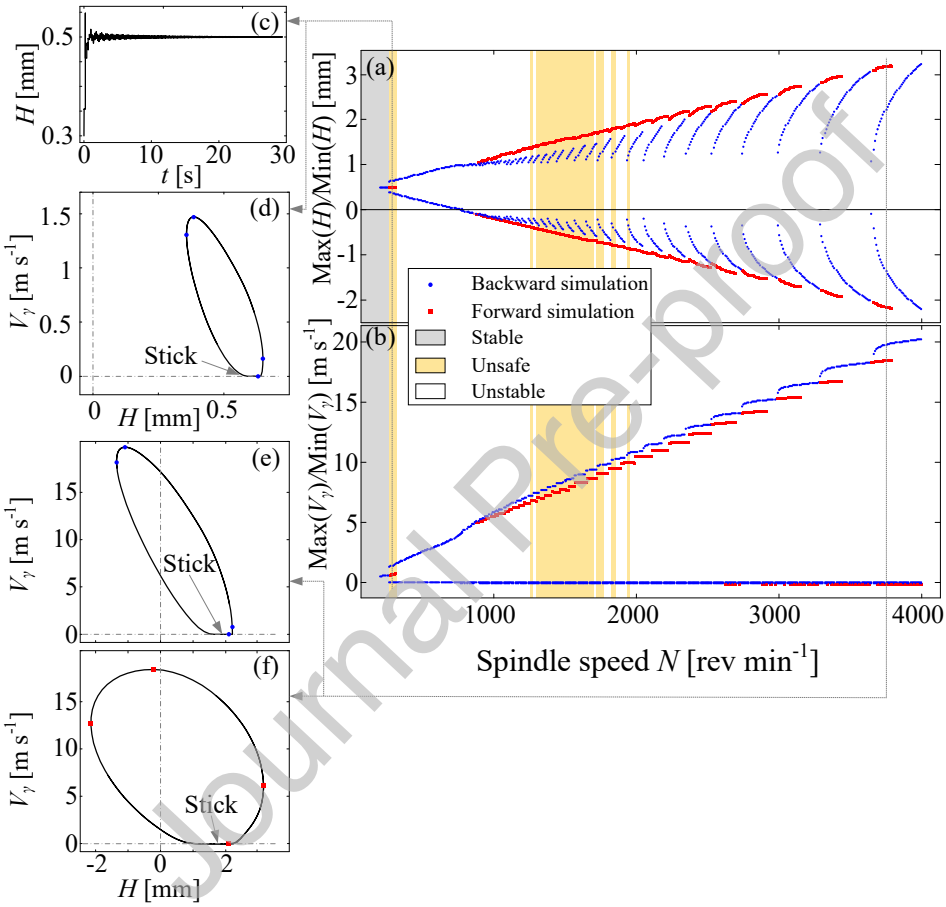

Figure 7: Bifurcation diagrams of (a) the depth of cut a_{p} and (b) frictional velocity V_γ as functions of spindle speed N for $a_{\mathrm{p}} = 1.4$ [mm], with time series of stationary cutting and (d) phase portraits of frictional chatter for $N = 300$ [rev min^{-1}] and (e-f) two coexisting chatter for $N = 3750$ [rev min^{-1}] added. The cutting dynamics in the low-velocity zone is dominated by the frictional chatter with non-smooth frictional velocity ($V_\gamma < 0$), while the regenerative chatter with non-smooth chip thickness ($H < 0$) becomes more and more important with respect to the increase of the spindle speed.

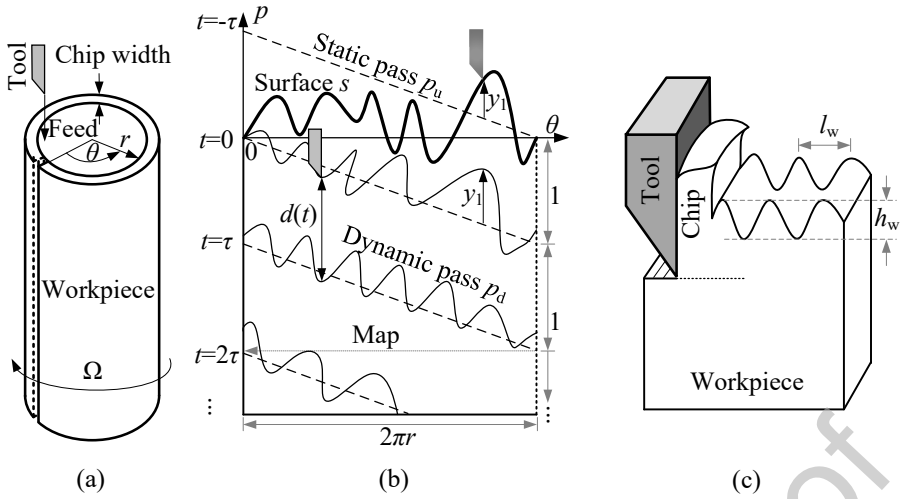

Figure 8: (a) The out-most layer of the cylindrical workpiece to be cut is mapped onto (b) the $\theta - p$ plane to represent the static and dynamics tool passes, p_u and p_d, with the initial surface s replotted in (c) to display the waviness height and length, l_w and h_w, in the original workpiece surface.

red squares represent the results obtained from backward (N decreases from 4000 [rev min^{-1}] to 200 [rev min^{-1}]) and forward (N increases from 200 [rev min^{-1}] to 4000 [rev min^{-1}]) simulations, respectively.

As can be seen in Fig. 7, the cutting is absolutely stable only for small spindle speed until N increases to 260 [rev min^{-1}] for the co-existence of stationary cutting and frictional chatter in the left-most UZ in Fig. 7. To illustrate, the stable cutting and frictional chatter for $N = 300$ [rev min^{-1}] are displayed in Figs 7(c) and (d). For $N > 330$ [rev min^{-1}], the instability features only a monostable frictional chatter until its amplitude is large enough to incur the loss of tool-workpiece contact at $N = 770$ [rev min^{-1}]. Thereafter, the cutting dynamics is dominated by multi-stability and the chatter motion keeps jumping among various periodic branches with its amplitude gradually increased. Corresponding with the branches for the large-amplitude frictional chatter shown in Figs 5 and 6, the co-existing vibrations for $N = 3750$ [rev min^{-1}] are displayed in Figs 7(e) and (f), respectively. Given the bifurcation diagrams shown in Figs 5 and 6, it is known that the frictional chatter in Fig. 7(e) will disappear immediately if a_p is decreased, leading to the bifurcation pattern similar to that in Fig. 5 showing the accurate estimation of UZ. On the contrary, the chatter in Fig. 7(f) persists with respect to the decrease of a_p, yielding a large UZ as shown in Fig. 6. Simply put, the "jump" among different large-amplitude frictional vibrations determines the co-existing cutting chatters in the UZs.

4. Safety estimation

In addition to the estimation of the size and location of UZs, cutting safety in the UZs is also very critical for global cutting stability. This is normally analysed by calculation of basin stability or basin of

attraction, indicating the percentage of initial conditions leading to various attractors [54, 55]. However, the initial spaces of time-delayed systems, such as the turning dynamics discussed here, have infinite many dimensions, so the calculation and visualization of their basins of attraction are very hard, if not impossible [37]. Thus next estimation of the cutting safety will use only the basin stability, i.e., the percentage of initial conditions leading to chatter, based on the approximate method proposed in [35, 42].

To this end, the outmost layer of the workpiece displayed in Fig. 8(a) is unfold and mapped onto the $\theta - p$ plane in Fig. 8(b), where the static and dynamic tools passes, p_{u} and p_{d}, are displayed as dashed and solid lines, respectively. Correspondingly, the difference between the two passes is the bending deformation of the tool in Y-direction:

$$y_1 = p_{\mathrm{d}} - p_{\mathrm{u}}. \tag{24}$$

Moreover, the initial surface waviness, s, can be regarded as a special dynamic pass left by a former manufacturing operation, thus the tool displacement before the tool cuts into the workpiece can be represented by

$$y_1(\tau) = s(\theta(\tau)) - p_{\mathrm{u}}(\theta(\tau)) \quad \theta(\tau) \in [0, 2\pi), \tag{25}$$

where $p_{\mathrm{u}}(\theta(\tau)) = 1 - \frac{\theta(\tau)}{2\pi}$ and $\theta(\tau) = 2\pi + \tau\Omega$ $(\tau \in [-\tau_{\mathrm{w}}, 0))$.

It is noted from Figs 8(a) and (b) that $s(\theta)$ is a periodic function with $s(0) = s(2\pi) = 0$, which can be represented by the following Fourier series [42]

$$\begin{aligned} s(\theta(\tau)) &\approx \sum_{i=1}^{N} a_i \left(\sin\left(i\theta + i\phi\right) - \sin\left(i\phi\right)\right) + \sum_{i=1}^{N} b_i \left(\cos\left(i\theta + i\phi\right) - \cos\left(i\phi\right)\right) \\ &= \sum_{i=1}^{N} a_i \left(\sin\left(i\Omega\tau + i\phi\right) - \sin\left(i\phi\right)\right) + \sum_{i=1}^{N} b_i \left(\cos\left(i\Omega\tau + i\phi\right) - \cos\left(i\phi\right)\right), \end{aligned} \tag{26}$$

where a_i and b_i depend on the waviness length and height (l_{w} and h_{w} in Fig. 8(c)) in the workpiece surface, and $\phi \in [0, 2\pi)$ reflects the geometry when the tool cuts into the workpiece [35]. For a limited waviness height, one can confine the selection of a_i and b_i by using a positive constraint parameter, α, for initial conditions [41] as follows

$$\sum_{i=1}^{N} a_i^2 + b_i^2 \leq \alpha^2. \tag{27}$$

In addition, another constraint parameter, β, is employed to restrict the strength of tool's initial free vibration as follows

$$y_1(0) \in [-\beta, \beta] \quad \text{and} \quad y_2(0) \in [-\beta, \beta]. \tag{28}$$

With the functional initial conditions approximated in Eq. (26), the basin stability of each co-

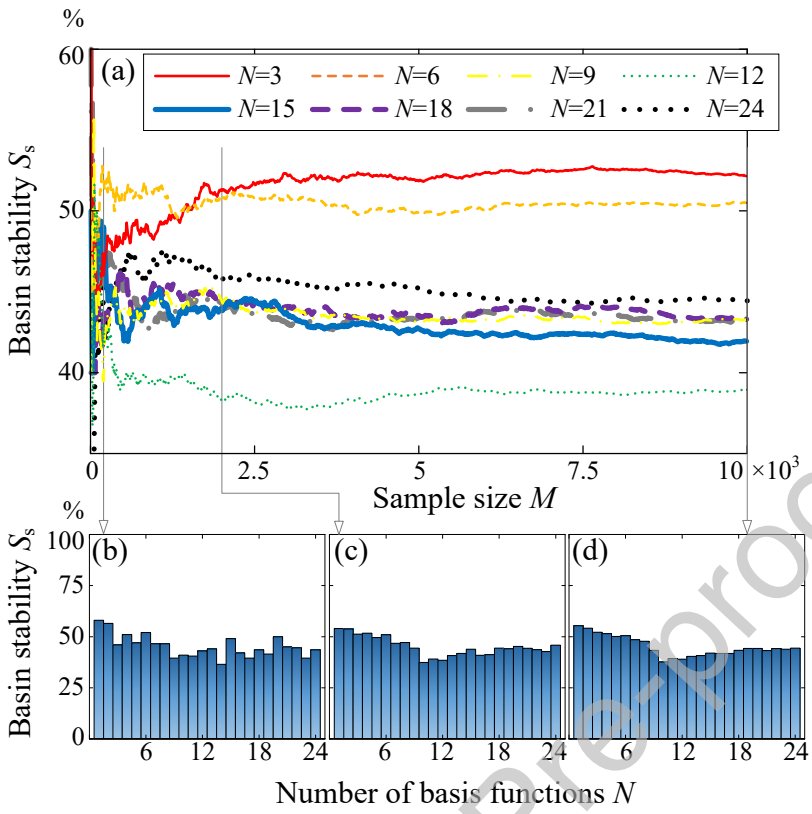

Figure 9: (a) With various numbers of harmonics for initial condition approximation, basin stabilities of stationary cutting, $S_{\rm s}$, for $N = 3600$ [rev min^{-1}] and $a_{\rm p} = 0.88$ [mm] are estimated and displayed as functions of the sample size. The influence of N on the estimation for (b) $M = 200$, (c) 2000 and (d) 10000 are added as well.

existing cutting dynamics can be estimated based on Monte Carlo principle, which randomly generates M groups of coefficients, $\{a_1^{(j)}, \cdots, a_n^{(j)}, b_1^{(j)}, \cdots, b_n^{(j)}, y_1(0)^{(j)}, y_2(0)^{(j)}, \phi^{(j)}\}_{j=1}^{M}$, to sample the functional initial space. By letting M_s, M_{sc} and M_{lc} respectively denote the numbers of initial conditions leading to stationary cutting, small- and large-amplitude chatters, the basin stabilities can be correspondingly estimated by

$$S_{\rm s} = \frac{M_{\rm s}}{M} \times 100\%, \quad S_{\rm sc} = \frac{M_{\rm sc}}{M} \times 100\%, \quad \text{and} \quad S_{\rm lc} = \frac{M_{\rm lc}}{M} \times 100\%. \tag{29}$$

When the sample size and the number of basis functions, M and N, are large enough, this estimation is anticipated to be convergent [42].

To illustrate the estimation of basin stability, the co-existing attractors displayed in Figs 4(c-e) for $N = 3600$ [rev min^{-1}] and $a_{\rm p} = 0.88$ [mm] are to be studied as an example. More specifically, constraints for the initial conditions, α and β, are fixed as 4 first, with the number of basis functions and sample size, N and M, gradually increasing from 1 until the convergence of estimation. Corresponding results in Fig. 9(a) displays $S_{\rm s}$ as functions of the sample size, which significantly oscillates at the beginning but convergent for $M \geq 2000$, no matter how many harmonics are chosen to approximate the initial functions.

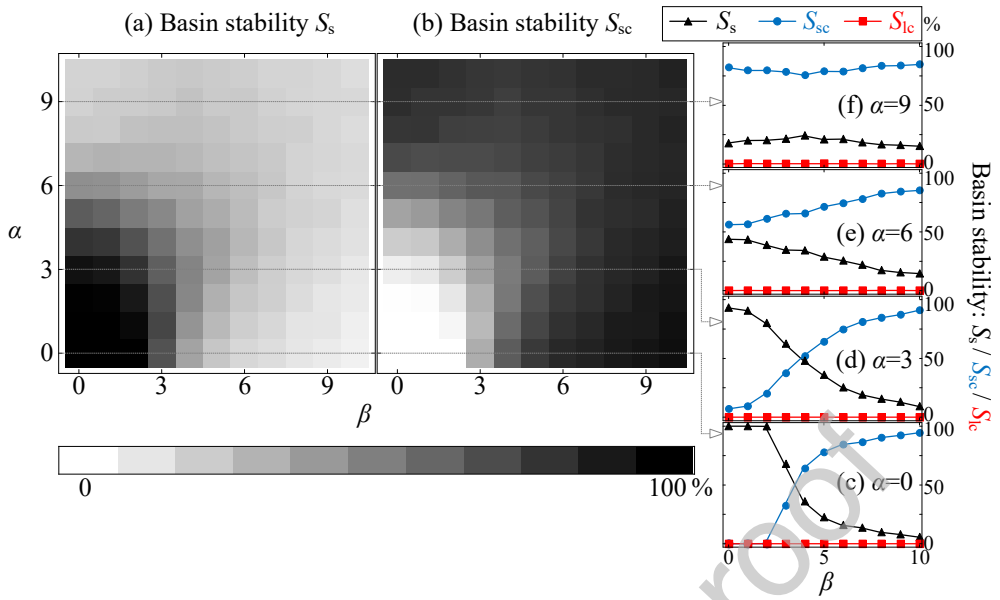

Figure 10: Influences of α and β on the basin stabilities of (a) stationary cutting and (b) small-amplitude chatter, with S_s, S_{sc} and S_{lc} displayed as functions of β for (c) $\alpha = 0$, (d) 3, (e) 6 and (f) 9. The increase of the constraints, α and β, makes the cutting process unsafer as the occurrence of small-amplitude chatter is increased, but the large-amplitude chatter hardly appears in this case.

In addition, the influence of N on the estimation is displayed in Figs 9(b-d), showing the convergence of S_s for $N > 18$ provided a large sample size ($M \geq 2000$) is used. Thus the following discussion will use $M = 2000$ and $N = 21$ for a valid estimation of basin stabilities.

Then the influences of the constraint parameters on the basin stability is studied with α and β selected in $[0, 10]$. As seen in Figs 10(a) and (b), larger constraints corresponding with rougher surfaces and stronger tool vibrations generally result in worse cutting safety, i.e., smaller basin stability of the stationary cutting, S_s, and larger possibility of the small-amplitude chatter, S_{sc}. The influence of β for $\alpha = 0$, 3, 6 and 9 are displayed in Figs 10(c-f), revealing that the large-amplitude chatter hardly occurs in practise as S_{lc} always stays around 0. For $\alpha = 0$ in Fig. 10(c), neither the large- nor the small-amplitude chatter shows up until the initial free tool vibration is strong enough ($\beta > 2$). For $\alpha = 3$ and 6 in Figs 10(d) and (e), the cutting safety keeps decreasing with respect to the increase of β as more and more initial conditions move towards the small-amplitude chatter. By contrast, Fig. 10(f) for $\alpha = 9$ is almost constant, with a local maximum of the cutting safety showing up for $\beta = 4$.

Finally, the cutting safety along the bifurcation diagram in Fig. 4 is estimated with various constraint parameters. The bifurcation diagram for $N = 3600$ [rev min^{-1}] is replotted in Fig. 11(a), showing a large unsafe zone for $a_p \in [0.82, 0.89]$ [mm]. Then the basin stabilities in this UZ are estimated for a small initial constraint ($\alpha = \beta = 1$), with S_s, S_{sc} and S_{lc} displayed as functions of a_p in Fig. 11(b). It is seen that the UZ from the statistical viewpoint is extremely small, as the possibility of chatter

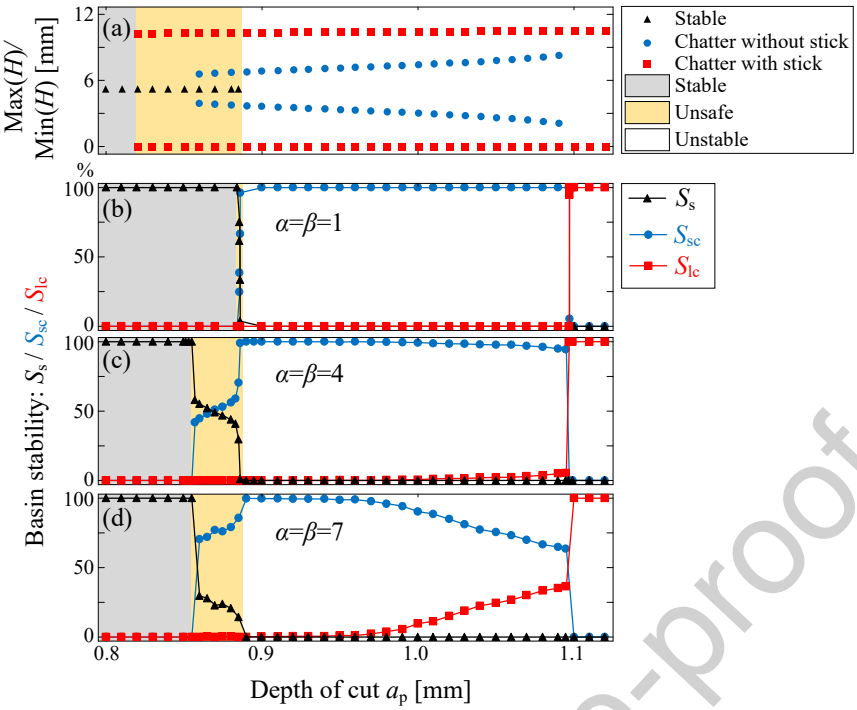

Figure 11: With the bifurcation diagram for $N = 3600$ [rev min^{-1}] enlarged in Panel (a), the basin stabilities are estimated for (b) $\alpha = \beta = 1$, (c) $\alpha = \beta = 4$, and (d) $\alpha = \beta = 7$, showing that a larger initial constraint leads to larger UZ and higher vibration energy but the large-amplitude frictional chatter has no influence on the UZ.

occurrence is non-zero only in a very small region close to the unstable zone. This result is in accordance to the "boundary layer" observed in [35, 42], demonstrating a high safety level in the UZ. By contrast, an intermediate initial constraint ($\alpha = \beta = 4$) significantly increases S_{sc}, but has no influence on S_{lc} in the UZ. The statistical UZ correspondingly expands leftwards, but does not enter the region without small-amplitude chatter. Similar result is obtained in Fig. 11(d) for a large initial constraint ($\alpha = \beta = 7$), showing an insignificant influence of the large-amplitude frictional chatter on the cutting safety. Besides, Figs 11(c) and (d) reveal that a stronger initial perturbation increases the occurrence of chatter with more energy, i.e. Fig. 11(d) has larger values of S_{sc} for $a_{\mathrm{p}} \in [0.86, 0.89]$ [mm] and of S_{lc} for $a_{\mathrm{p}} \in [0.97, 1.1]$ [mm] compared with Fig. 11(c). This confirms the obvious from the metal cutting knowledge that a fine workpiece surface and a static tool result in a better cutting safety.

5. Conclusions

Based on our previous modelling and analysis of regenerative and frictional cutting dynamics, we have explored nonlinear cutting dynamics with efforts specially put on multi-stability. With the UZs located by analytical and numerical bifurcation analyses and the functional initial conditions approximated by Fourier series, the cutting safety has been estimated by basin stability, revealing the relationship between

initial constraints and the possibility of chatter occurrence.

Perturbation analysis unveiled subcritical instabilities of the linear stability boundaries, demonstrating multi-stability in the linearly stable region adjacent to the boundaries (UZs). However, the additional nonlinearity and non-smoothness introduced by the chip-tool friction significantly influences the bistability near linear stability boundaries, resulting in an invalid estimation of the UZ by the perturbation method. We resolved this problem by the numerical bifurcation analysis and an extended UZ induced by the persistence of large-amplitude frictional chatter in the linearly stable region, was determined. Thus the size of the UZ estimated by the perturbation method could be qualitatively valid only for the chatter with no sticking phases resulting form frictional interactions.

To further assess the cutting safety in the UZs, Fourier series and Monte Carlo principle were used to approximate the functional initial conditions, with the waviness height, cutting geometry and initial tool deformation randomly generated to estimate the basin stabilities of stationary cutting, small- and large-amplitude chatters, respectively. This estimation gradually converged when more and more samples and basis functions were used.

It was then revealed that the influence of large-amplitude chatter on the UZ is insignificant from the statistical viewpoint. The cutting dynamics never jumped onto this orbit when it co-exists with the stable stationary cutting, showing that the UZ estimation by perturbation method is statistically valid.

Appendix A. Continuation scheme

Section 2.2 employs a numerical continuation scheme solve the transcendental eigenvalue equation, Eq. (20), to locate the critical boundaries for the cutting stability. As illustrated in Fig. A.1, this method requires two initial solutions for the guess of their adjacent solution, which is used to start the Newton-Raphson iteration for the new solution. If the iteration fails to convergent, a new guess will be given with the relaxing parameter, r, decreased. This procedure is be repeated until the boundary of interested parameter regions is reached or the number of solutions is more than the pre-defined maximum step.

Appendix B. Nonlinear analysis by MMS

To track the periodic branch born on the stability boundary for the UZs, the method of multiple scales (MMS) is adopted [52]. To begin with, the dimensionless depth of cut, w, is detuned into

$$w = w_c + \epsilon^2 w_\epsilon, \tag{B.1}$$

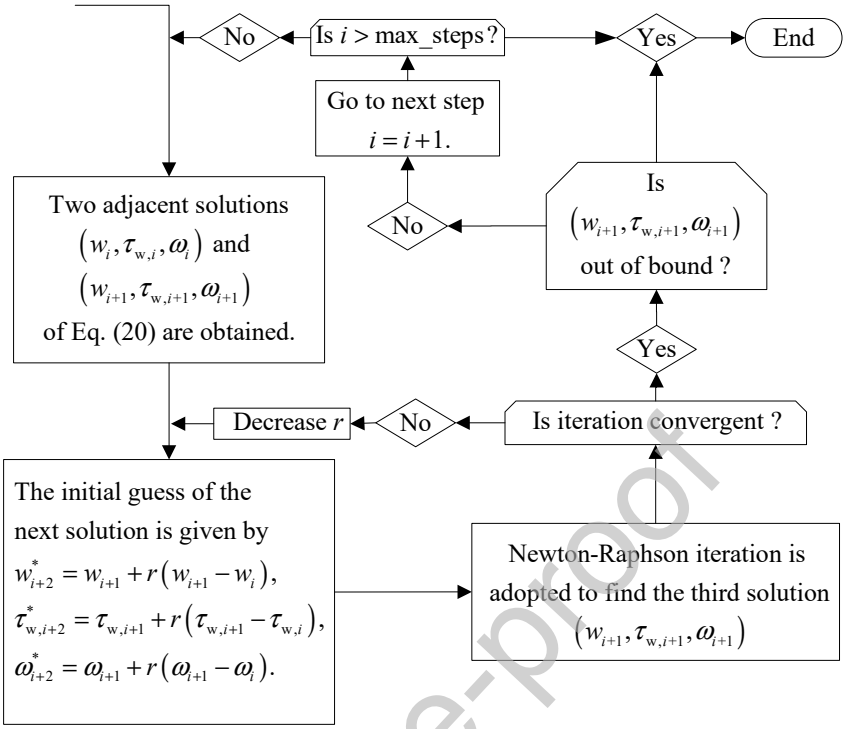

Figure A.1: Numerical continuation scheme for continuously solving Eq. (20), yielding the stability boundaries in Fig. 2.

where w_c is the critical depth of cut on the boundaries, and ϵ is a bookkeeping dimensionless parameter indicating that w is in the neighbourhood of w_c. Then $T_0 = \tau$ and a slow time scale $T_2 = \epsilon^2\tau$, are introduced with the solution of (Eq. 12) expanded into

$$\begin{aligned}\mathbf{y}(\tau) &= \epsilon \mathbf{y}_1(T_0, T_2) + \epsilon^2 \mathbf{y}_2(T_0, T_2) + \epsilon^3 \mathbf{y}_3(T_0, T_2) + \cdots \\ &= \epsilon \begin{pmatrix} y_{11}(T_0, T_2) \\ y_{21}(T_0, T_2) \end{pmatrix} + \epsilon^2 \begin{pmatrix} y_{12}(T_0, T_2) \\ y_{22}(T_0, T_2) \end{pmatrix} + \epsilon^3 \begin{pmatrix} y_{13}(T_0, T_2) \\ y_{23}(T_0, T_2) \end{pmatrix} + \cdots .\end{aligned} \tag{B.2}$$

Correspondingly, the delayed term is expanded into

$$\begin{aligned} y_1(\tau - \tau_w) =& \epsilon y_{11}(T_0 - \tau_w, T_2 - \epsilon^2\tau_w) + \epsilon^2 y_{12}(T_0 - \tau_w, T_2 - \epsilon^2\tau_w) \\ &+ \epsilon^3 y_{13}(T_0 - \tau_w, T_2 - \epsilon^2\tau_w) + \cdots \\ =& \epsilon y_{11}(T_0 - \tau_w, T_2) + \epsilon^2 y_{12}(T_0 - \tau_w, T_2) \\ &+ \epsilon^3 \left(y_{13}(T_0 - \tau_w, T_2) - \tau \frac{\partial y_{11}(T_0 - \tau_w, T_2)}{\partial T_2} \right) + \cdots . \end{aligned} \tag{B.3}$$

Then, substituting Eqs (B.1), (B.2) and (B.3) into Eq. (12) and collecting the coefficients of ϵ and ϵ^2

yield

$$\begin{aligned}
&\frac{\partial y_{11}}{\partial T_0} - y_{21} = 0,\\
&\frac{\partial y_{21}}{\partial T_0} + y_{11} + \xi y_{21} + w_{\mathrm{c}}\left(\mu_{\mathrm{d}}\cos(\gamma) + (\mu_{\mathrm{s}} - \mu_{\mathrm{d}})\,\mathrm{e}^{-\frac{60}{v_{\mathrm{s}}\tau_{\mathrm{w}}}}\cos(\gamma) - \sin(\gamma)\right)(y_{11} - y_{11\tau})\\
&\quad + w_{\mathrm{c}}\left(c_y\frac{\tau_{\mathrm{w}}}{60} - (\mu_{\mathrm{s}} - \mu_{\mathrm{d}})\mathrm{e}^{-\frac{60}{v_{\mathrm{s}}\tau_{\mathrm{w}}}}\nu\cos^2(\gamma)\right)y_{21} = 0,
\end{aligned} \tag{B.4}$$

and

$$\begin{aligned}
&\frac{\partial y_{12}}{\partial T_0} - y_{22} = 0,\\
&\frac{\partial y_{22}}{\partial T_0} + y_{12} + \xi y_{22} + w_{\mathrm{c}}\left(\mu_{\mathrm{d}}\cos(\gamma) + (\mu_{\mathrm{s}} - \mu_{\mathrm{d}})\,\mathrm{e}^{-\frac{60}{v_{\mathrm{s}}\tau_{\mathrm{w}}}}\cos(\gamma) - \sin(\gamma)\right)(y_{12} - y_{12\tau})\\
&\quad + w_{\mathrm{c}}\left(c_y\frac{\tau_{\mathrm{w}}}{60} - (\mu_{\mathrm{s}} - \mu_{\mathrm{d}})\mathrm{e}^{-\frac{60}{v_{\mathrm{s}}\tau_{\mathrm{w}}}}\nu\cos^2(\gamma)\right)y_{22}\\
&= w_{\epsilon}\left(\mu_{\mathrm{d}}\cos(\gamma) + (\mu_{\mathrm{s}} - \mu_{\mathrm{d}})\,\mathrm{e}^{-\frac{60}{v_{\mathrm{s}}\tau_{\mathrm{w}}}}\cos(\gamma) - \sin(\gamma)\right)\\
&\quad - w_{\mathrm{c}}(\mu_{\mathrm{s}} - \mu_{\mathrm{d}})\mathrm{e}^{-\frac{60}{v_{\mathrm{s}}\tau_{\mathrm{w}}}}\nu\cos^2(\gamma)(y_{11} - y_{11\tau})y_{21} + \frac{w_{\mathrm{c}}}{2}(\mu_{\mathrm{s}} - \mu_{\mathrm{d}})\mathrm{e}^{-\frac{60}{v_{\mathrm{s}}\tau_{\mathrm{w}}}}\nu^2\cos^3(\gamma)y_{21}^2,
\end{aligned} \tag{B.5}$$

where $y_{ij} = y_{ij}(T_0, T_2)$ and $y_{1i\tau} = y_{1j}(T_0 - \tau, T_2)$ ($i = 1, 2$ and $j = 1, 2, 3, \cdots$). As Eq. (B.4) corresponds with Eq. (15), it has the non-decaying solution

$$\mathbf{y}_1 = \begin{pmatrix} y_{11} \\ y_{21} \end{pmatrix} = \begin{pmatrix} r_1 \\ r_2 \end{pmatrix} A(T_2)\mathrm{e}^{\mathrm{i}\omega T_0} + \text{c.c.} \tag{B.6}$$

where c.c. is the complex conjugate of its preceding terms, and $(r_1, r_2)^{\mathrm{T}} = (1, \mathrm{i}\omega)^{\mathrm{T}}$ denotes a right eigenvector with respect to the critical eigenvalue $\lambda = \pm\mathrm{i}\omega$. Substituting Eq. (B.6) into Eq. (B.4) yields

$$\begin{aligned}
&\frac{\partial y_{12}}{\partial T_0} - y_{22} = 0,\\
&\frac{\partial y_{22}}{\partial T_0} + y_{12} + \xi y_{22} + w_{\mathrm{c}}\left(\mu_{\mathrm{d}}\cos(\gamma) + (\mu_{\mathrm{s}} - \mu_{\mathrm{d}})\,\mathrm{e}^{-\frac{60}{v_{\mathrm{s}}\tau_{\mathrm{w}}}}\cos(\gamma) - \sin(\gamma)\right)(y_{12} - y_{12\tau})\\
&\quad + w_{\mathrm{c}}\left(c_y\frac{\tau_{\mathrm{w}}}{60} - (\mu_{\mathrm{s}} - \mu_{\mathrm{d}})\mathrm{e}^{-\frac{60}{v_{\mathrm{s}}\tau_{\mathrm{w}}}}\nu\cos^2(\gamma)\right)y_{22}\\
&= w_{\epsilon}\left(\mu_{\mathrm{d}}\cos(\gamma) + (\mu_{\mathrm{s}} - \mu_{\mathrm{d}})\,\mathrm{e}^{-\frac{60}{v_{\mathrm{s}}\tau_{\mathrm{w}}}}\cos(\gamma) - \sin(\gamma)\right)\\
&\quad - w_{\mathrm{c}}(\mu_{\mathrm{s}} - \mu_{\mathrm{d}})\mathrm{e}^{-\frac{60}{v_{\mathrm{s}}\tau_{\mathrm{w}}}}\nu\cos^2(\gamma)(1 - \mathrm{e}^{-\mathrm{i}\omega\tau_{\mathrm{w}}})\mathrm{i}\omega(A(T_2)^2\mathrm{e}^{2\mathrm{i}\omega T_0} - A(T_2)\overline{A}(T_2))\\
&\quad + \frac{w_{\mathrm{c}}}{2}(\mu_{\mathrm{s}} - \mu_{\mathrm{d}})\mathrm{e}^{-\frac{60}{v_{\mathrm{s}}\tau_{\mathrm{w}}}}\nu^2\cos^3(\gamma)\omega^2(A(T_2)\overline{A}(T_2) - A(T_2)^2\mathrm{e}^{2\mathrm{i}\omega T_0}) + \text{c.c.},
\end{aligned} \tag{B.7}$$

where $\overline{\bullet}$ denotes the complex conjugate of $\bullet$. For brevity, we introduce

$$\begin{aligned}\mathbf{C}_0 &= -\mathbf{A} - \mathbf{D},\\ \mathbf{C}_2 &= 2\mathrm{i}\omega\mathbf{I} - \mathbf{A} - \mathbf{D}\mathrm{e}^{-\mathrm{i}2\omega\tau_\mathrm{w}},\end{aligned} \tag{B.8}$$

and

$$\begin{aligned}\chi_0 =& w_\epsilon\left(\mu_\mathrm{d}\cos(\gamma) + (\mu_\mathrm{s}-\mu_\mathrm{d})\,\mathrm{e}^{-\frac{60}{v_\mathrm{s}\tau_\mathrm{w}}}\cos(\gamma) - \sin(\gamma)\right)\\ &- w_\mathrm{c}(\mu_\mathrm{s}-\mu_\mathrm{d})\mathrm{e}^{-\frac{60}{v_\mathrm{s}\tau_\mathrm{w}}}\nu\cos^2(\gamma)(1-\mathrm{e}^{-\mathrm{i}\omega\tau_\mathrm{w}})\mathrm{i}\omega(-A(T_2)\overline{A}(T_2))\\ &+ \frac{w_\mathrm{c}}{2}(\mu_\mathrm{s}-\mu_\mathrm{d})\mathrm{e}^{-\frac{60}{v_\mathrm{s}\tau_\mathrm{w}}}\nu^2\cos^3(\gamma)\omega^2 A(T_2)\overline{A}(T_2) + \mathrm{c.c.},\\ \chi_2 =& - w_\mathrm{c}(\mu_\mathrm{s}-\mu_\mathrm{d})\mathrm{e}^{-\frac{60}{v_\mathrm{s}\tau_\mathrm{w}}}\nu\cos^2(\gamma)(1-\mathrm{e}^{-\mathrm{i}\omega\tau_\mathrm{w}})\mathrm{i}\omega A(T_2)^2\mathrm{e}^{2\mathrm{i}\omega T_0}\\ &+ \frac{w_\mathrm{c}}{2}(\mu_\mathrm{s}-\mu_\mathrm{d})\mathrm{e}^{-\frac{60}{v_\mathrm{s}\tau_\mathrm{w}}}\nu^2\cos^3(\gamma)\omega^2(-A(T_2)^2\mathrm{e}^{2\mathrm{i}\omega T_0}) + \mathrm{c.c.},\end{aligned} \tag{B.9}$$

to represent the particular solution of Eq. (B.7) as follows

$$\mathbf{y}_2 = \begin{pmatrix} y_{12}\\ y_{22}\end{pmatrix} = \mathbf{C}_0^{-1}\begin{pmatrix} 0\\ \chi_0\end{pmatrix} + \mathbf{C}_2^{-1}\begin{pmatrix} 0\\ \chi_2\end{pmatrix} + \mathrm{c.c.}. \tag{B.10}$$

Next, substituting Eqs (B.1), (B.2), (B.3), (B.6) and (B.10) into Eq. (12), collecting the coefficients of ϵ^3 and eliminating the secular terms which are proportional to $\mathrm{e}^{\mathrm{i}\omega T_0}$ by Fredholm Alternative [52], one can obtain the governing equation of $A(T_2)$ as

$$\frac{\partial A(T_2)}{\partial T_2} = \Lambda_1 A(T_2) + \Lambda_3 A(T_2)^2\overline{A}(T_2), \tag{B.11}$$

where Λ_1 and Λ_3 depend on all of the dimensionless parameters. Their detailed expressions are omitted here as they are too tedious. Lastly, substituting $A(T_2)$ obtained by solving Eq. (B.11) in Eq. (B.6) yields the first order approximation of the periodic chatter, following which one can estimate the UZs shown in Fig. 3(a) by checking the non-smoothness in the cutting depth [34].

Acknowledgements

This research is supported by National Natural Science Foundation of China (Grants No. 11872147, 12072068, 11932015 and 11502048).

References

[1] T. G. Molnár, Z. Dombovari, T. Insperger, G. Stépán, On the analysis of the double hopf bifurcation in machining processes via centre manifold reduction, Proceedings of the Royal Society A: Mathematical, Physical and Engineering Science 473 (2207) (2017) 1–20. doi:10.1098/rspa.2017.0502.

[2] R. Rusinek, M. Wiercigroch, P. Wahi, Modelling of frictional chatter in metal cutting, International Journal of Mechanical Sciences 89 (0) (2014) 167–176. doi:10.1016/j.ijmecsci.2014.08.020.

[3] Y. Altintas, M. Eynian, H. Onozuka, Identification of dynamic cutting force coefficients and chatter stability with process damping, CIRP Annals 57 (1) (2008) 371–374. doi:10.1016/j.cirp.2008.03.048.

[4] M. Wiercigroch, Chaotic vibration of a simple model of the machine tool-cutting process system, Journal of Vibration and Acoustics 119 (3) (1997) 468–475. doi:10.1115/1.2889747.

[5] J. Rech, P. J. Arrazola, C. Claudin, C. Courbon, F. Pusavec, J. Kopac, Characterisation of friction and heat partition coefficients at the tool-work material interface in cutting, CIRP Annals 62 (1) (2013) 79–82. doi:10.1016/j.cirp.2013.03.099.

[6] W. Bai, R. Sun, A. Roy, V. V. Silberschmidt, Improved analytical prediction of chip formation in orthogonal cutting of titanium alloy ti6al4v, International Journal of Mechanical Sciences 133 (2017) 357–367. doi:10.1016/j.ijmecsci.2017.08.054.

[7] Y. Yan, J. Xu, M. Wiercigroch, Modelling of regenerative and frictional cutting dynamics, International Journal of Mechanical Sciences 156 (2019) 86–93. doi:10.1016/j.ijmecsci.2019.03.032.

[8] Z. Fu, X. Zhang, X. Wang, W. Yang, Analytical modeling of chatter vibration in orthogonal cutting using a predictive force model, International Journal of Mechanical Sciences 88 (2014) 145–153. doi:10.1016/j.ijmecsci.2014.08.005.

[9] K. Kecik, R. Rusinek, J. Warminski, Modeling of high-speed milling process with frictional effect, Proceedings of the Institution of Mechanical Engineers, Part K: Journal of Multi-body Dynamics 227 (1) (2013) 3–11. doi:10.1177/1464419312458636.

[10] R. Rusinek, K. Kecik, J. Warminski, A. Weremczuk, Dynamic model of cutting process with modulated spindle speed, AIP Conference Proceedings 1493 (1) (2012) 805–809. doi:10.1063/1.4765580.

[11] A. Weremczuk, R. Rusinek, Influence of frictional mechanism on chatter vibrations in the cutting processanalytical approach, The International Journal of Advanced Manufacturing Technology 89 (9) (2017) 2837–2844. doi:10.1007/s00170-016-9520-5.

[12] M. Wiercigroch, E. Budak, Sources of nonlinearities, chatter generation and suppression in metal cutting, Philosophical Transactions of the Royal Society of London. Series A: Mathematical, Physical and Engineering Sciences 359 (1781) (2001) 663–693. doi:10.1098/rsta.2000.0750.

[13] G. Stépán, Modelling nonlinear regenerative effects in metal cutting, Philosophical Transactions of the Royal Society of London. Series A: Mathematical, Physical and Engineering Sciences 359 (1781) (2001) 739 –757. doi:10.1098/rsta.2000.0753.

[14] J. R. Pratt, A. H. Nayfeh, Chatter control and stability analysis of a cantilever boring bar under regenerative cutting conditions, Philosophical Transactions of the Royal Society of London. Series A: Mathematical, Physical and Engineering Sciences 359 (2001) 759–792. doi:10.1098/rsta.2000.0754.

[15] X. Long, P. Zheng, S. Ren, Active delayed control of turning and milling dynamics, Journal of Computational and Nonlinear Dynamics 12 (5) (2017) 051022. doi:10.1115/1.4036913.

[16] J. Jung, P. Kim, H. Kim, J. Seok, Dynamic modeling and simulation of a nonlinear, non-autonomous grinding system considering spatially periodic waviness on workpiece surface, Simulation Modelling Practice and Theory 57 (2015) 88–99. doi:10.1016/j.simpat.2015.06.005.

[17] Y. Yan, M. Wiercigroch, Dynamics of rotary drilling with non-uniformly distributed blades, International Journal of Mechanical Sciencesdoi:https://doi.org/10.1016/j.ijmecsci.2019.05.016.

[18] M. Wiercigroch, A. M. Krivtsov, Frictional chatter in orthogonal metal cutting, Philosophical Transactions of the Royal Society of London A: Mathematical, Physical and Engineering Sciences 359 (1781) (2001) 713–738. doi:10.1098/rsta.2000.0752.

[19] R. Rusinek, M. Wiercigroch, P. Wahi, Influence of tool flank forces on complex dynamics of cutting process, International Journal of Bifurcation and Chaos 24 (09) (2014) 1450115. doi:10.1142/S0218127414501156.

[20] Y. Yan, J. Xu, M. Wiercigroch, Regenerative and frictional chatter in plunge grinding, Nonlinear Dynamics 86 (1) (2016) 283–307. doi:10.1007/s11071-016-2889-8.

[21] Y. Liu, J. Pez Chvez, R. De Sa, S. Walker, Numerical and experimental studies of stickslip oscillations in drill-strings, Nonlinear Dynamics 90 (4) (2017) 2959–2978. doi:10.1007/s11071-017-3855-9.

[22] Y. Altintas, M. Weck, Chatter stability of metal cutting and grinding, CIRP Annals - Manufacturing Technology 53 (2) (2004) 619–642. doi:10.1016/S0007-8506(07)60032-8.

[23] S. Zhang, J. Xu, K.-w. Chung, Desynchronization-based congestion suppression for a star-type internet system with arbitrary dimension, Neurocomputingdoi:10.1016/j.neucom.2017.05.023.

[24] X. Sun, J. Xu, J. Fu, The effect and design of time delay in feedback control for a nonlinear isolation system, Mechanical Systems and Signal Processing 87 (Part A) (2017) 206–217. doi:https://doi.org/10.1016/j.ymssp.2016.10.022.

[25] K. Lu, Z. Lian, F. Gu, H. Liu, Model-based chatter stability prediction and detection for the turning of a flexible workpiece, Mechanical Systems and Signal Processing 100 (Supplement C) (2018) 814–826. doi:10.1016/j.ymssp.2017.08.022.

[26] D. Smolenicki, J. Boos, F. Kuster, H. Roelofs, C. F. Wyen, In-process measurement of friction coefficient in orthogonal cutting, CIRP Annals 63 (1) (2014) 97–100. doi:10.1016/j.cirp.2014.03.083.

[27] J. M. Allwood, T. H. C. Childs, A. T. Clare, A. K. M. De Silva, V. Dhokia, I. M. Hutchings, R. K. Leach, D. R. Leal-Ayala, S. Lowth, C. E. Majewski, A. Marzano, J. Mehnen, A. Nassehi, E. Ozturk, M. H. Raffles, R. Roy, I. Shyha, S. Turner, Manufacturing at double the speed, Journal of Materials Processing Technology 229 (2016) 729–757. doi:10.1016/j.jmatprotec.2015.10.028.

[28] E. Türkeş, S. Neşeli, A simple approach to analyze process damping in chatter vibration, The International Journal of Advanced Manufacturing Technology 70 (5) (2014) 775–786. doi:10.1007/s00170-013-5307-0.

[29] E. Türkeş, S. Orak, S. Neşeli, M. Sahin, S. Selvi, Modelling of dynamic cutting force coefficients and chatter stability dependent on shear angle oscillation, The International Journal of Advanced Manufacturing Technology 91 (1) (2017) 679–686. doi:10.1007/s00170-016-9782-y.

[30] Y. Yan, J. Xu, M. Wiercigroch, Stability and dynamics of parallel plunge grinding, The International Journal of Advanced Manufacturing Technology 99 (1) (2018) 881–895. doi:10.1007/s00170-018-2440-9.

[31] T. Insperger, D. A. W. Barton, G. Stépán, Criticality of hopf bifurcation in state-dependent delay model of turning processes, International Journal of Non-Linear Mechanics 43 (2) (2008) 140–149. doi:10.1016/j.ijnonlinmec.2007.11.002.

[32] Z. Dombovari, R. E. Wilson, G. Stepan, Estimates of the bistable region in metal cutting, Proceedings of the Royal Society A: Mathematical, Physical and Engineering Science 464 (2100) (2008) 3255–3271. doi:10.1098/rspa.2008.0156.

[33] Z. Dombovari, G. Stepan, On the bistable zone of milling processes, Philosophical Transactions of the Royal Society A: Mathematical, Physical and Engineering Sciences 373 (2051) (2015) 1–17. doi:10.1098/rsta.2014.0409.

[34] T. G. Molnár, T. Insperger, S. J. Hogan, G. Stépán, Estimation of the bistable zone for machining operations for the case of a distributed cutting force model, ASME Journal of Computational and Nonlinear Dynamics 11 (2016) 051008. doi:10.1115/1.4032443.

[35] Y. Yan, J. Xu, M. Wiercigroch, Basins of attraction of the bistable region of time-delayed cutting dynamics, Physical Review E 96 (3) (2017) 032205. doi:10.1103/PhysRevE.96.032205.

[36] Y. Liu, J. Páez Chávez, Controlling multistability in a vibro-impact capsule system, Nonlinear Dynamics (2017) 1–16doi:10.1007/s11071-016-3310-3.

[37] J. Hale, Theory of Functional Differential Equations, Springer-Verlag, New York, 1977.

[38] H. Shang, Pull-in instability of a typical electrostatic mems resonator and its control by delayed feedback, Nonlinear Dynamics 90 (1) (2017) 171–183. doi:10.1007/s11071-017-3653-4.

[39] J. C. Ji, Two families of super-harmonic resonances in a time-delayed nonlinear oscillator, Journal of Sound and Vibration 349 (2015) 299–314. doi:10.1016/j.jsv.2015.03.049.

[40] H. Wang, H. Hu, Z. Wang, Global dynamics of a duffing oscillator with delayed displacement feedback, International Journal of Bifurcation and Chaos 14 (08) (2004) 2753–2775. doi:10.1142/S0218127404010990.

[41] S. Leng, W. Lin, J. Kurths, Basin stability in delayed dynamics, Scientific Reports 6 (2016) 21449. doi:dx.doi.org/10.1038/srep21449.

[42] Y. Yan, J. Xu, M. Wiercigroch, Estimation and improvement of cutting safety, Nonlinear Dynamicsdoi:10.1007/s11071-019-04980-0.

[43] G. Stépán, A. K. Kiss, B. Ghalamchi, J. Sopanen, D. Bachrathy, Chatter avoidance in cutting highly flexible workpieces, CIRP Annals 66 (1) (2017) 377–380. doi:10.1016/j.cirp.2017.04.054.

[44] S. Bahi, G. List, G. Sutter, Analysis of adhered contacts and boundary conditions of the secondary shear zone, Wear 330-331 (2015) 608–617. doi:10.1016/j.wear.2015.01.016.

[45] F. Zhou, A new analytical tool-chip friction model in dry cutting, The International Journal of Advanced Manufacturing Technology 70 (1) (2014) 309–319. doi:10.1007/s00170-013-5271-8.

[46] W. F. Hastings, P. Mathew, P. L. B. Oxley, A machining theory for predicting chip geometry, cutting forces etc. from work material properties and cutting conditions, Proceedings of the Royal Society of London. A. Mathematical and Physical Sciences 371 (1747) (1980) 569 –587.

[47] Y. Liu, E. Pavlovskaia, D. Hendry, M. Wiercigroch, Vibro-impact responses of capsule system with various friction models, International Journal of Mechanical Sciences 72 (0) (2013) 39–54. doi:10.1016/j.ijmecsci.2013.03.009.

[48] Y. Yan, Y. Liu, M. Liao, A comparative study of the vibro-impact capsule systems with one-sided and two-sided constraints, Nonlinear Dynamics 89 (2) (2017) 1063–1087. doi:10.1007/s11071-017-3500-7.

[49] Y. Yan, J. Xu, M. Wiercigroch, Regenerative chatter in a plunge grinding process with workpiece imbalance, The International Journal of Advanced Manufacturing Technology 89 (9) (2017) 2845–2862. doi:10.1007/s00170-016-9830-7.

[50] M. Eynian, Chatter stability of turning and milling with process damping, Ph.D. thesis, The University of British Columbia (2010).

[51] C. Claudin, A. Mondelin, J. Rech, G. Fromentin, Effects of a straight oil on friction at the tool-workmaterial interface in machining, International Journal of Machine Tools and Manufacture 50 (8) (2010) 681–688. doi:10.1016/j.ijmachtools.2010.04.013.

[52] A. H. Nayfeh, Order reduction of retarded nonlinear systems - the method of multiple cales versus center-manifold reduction, Nonlinear Dynamics 51 (2008) 483–500. doi:10.1007/s11071-007-9237-y.

[53] Y. Yan, J. Xu, M. Wiercigroch, Non-linear analysis and quench control of chatter in plunge grinding, International Journal of Non-Linear Mechanics 70 (2015) 134–144. doi:10.1016/j.ijnonlinmec.2014.06.012.

[54] P. Belardinelli, S. Lenci, Improving the global analysis of mechanical systems via parallel computation of basins of attraction, Procedia IUTAM 22 (2017) 192–199. doi:10.1016/j.piutam.2017.08.028.

[55] K. Yadav, A. Prasad, M. D. Shrimali, Control of coexisting attractors via temporal feedback, Physics Letters A 382 (32) (2018) 2127–2132. doi:https://doi.org/10.1016/j.physleta.2018.05.041.

Declaration of Competing Interest

The authors declare that they have no known competing financial interests or personal relationships that could have appeared to influence the work reported in this paper.

Credit Author Statment

Yao Yan: Methodology, Software, Formal analysis, Writing - original draft.

Guojun Liu: Visualization, Data Curation.

Marian Wiercigroch: Conceptualization, Writing - review & editing.

Jian Xu: Supervision, Project administration, Funding acquisition.